Computational studies of the bulk cobalt pentlandite (Co_9S_8): Validation of the potential model.

M.A. Mehlape[1], P.E. Ngoepe[1] and S.C. Parker[2]

1. Materials Modelling Centre, School of Physical and Mineral Sciences, University of Limpopo, South Africa, Private Bag, X1106, SOVENGA, 0727
2. Computational Solid State Chemistry, University of Bath, Claverton Down, Bath, Avon, UK BA2 7AY.

Email:mofuti.mehlape@ul.ac.za

Abstract. We use the density functional theory to study the cobalt pentlandite mineral, (Co_9S_8). We investigate various forms of the cobalt pentlandite, Co_9S_8, at different temperatures, using classical atomistic simulation methods with the support of electronic structure calculations. The first interatomic potentials of Co_9S_8 based on the Born model, were derived with input data such as structure and elastic properties from experiments and electronic structure calculations respectively. The interatomic potentials were validated by running energy minimization and molecular dynamics calculations. The structure and elastic properties corresponded well with those determined by electronic structure methods. The calculations further reproduced the complex high temperature transformation to high form pentlandite and the melting of Co_9S_8; as deduced from the crystal structure and radial distribution functions.

1. Introduction

Pentlandites, $(Fe,Ni,Co)_9S_8$, are important nickel and cobalt sulphide minerals in economic deposits where it occurs with pyrrohotite, chalcopyrite and pyrite in mafic and ultramafic igneous rocks [1]. Furthermore, pentlandite minerals play an important role in the production of cleaner fuels with low or ultra-low sulphur content that require a continuous improvement of catalytic materials used in the refinement industry. In addition to supplying base metals, pentlandite compounds occur as solid solutions, in Merenksy reef, and intergrowths in UG2 reefs, with precious metal compounds, where the former occur in larger quantities [2]. In order to extract the precious metals from the ores effectively it is necessary to study and understand structural, including surface properties, of pentlandites in detail. Notwithstanding their significance in mineralogy, previous experimental studies on pentlandites are not as abundant as those of pyrites and metal oxide minerals, and computational modelling investigations are also very scarce. We present the first classical interatomic potential model [3] of Co_9S_8, and its validation, since the compound is easier to handle than $(Fe, Ni)_9S_8$, owing to its cubic symmetry. Such potentials render structural studies of surfaces and nanoparticles, with large number of atoms, and their variation with temperature more amenable.

2.1. Cobalt Pentlandite, Co_9S_8 structure

The conventional unit cell of the cobalt pentlandite has the formula $Co_{36}S_{32}$ and contains a cubic close-packed arrangement of sulphide ions containing 64 tetrahedral holes and 32 octahedral holes. Of the 64 tetrahedral holes, 32 are occupied by Co^{2+} ions, these being distributed through the lattice in groups of eight which lie at the corners of sub-cubes of edge length 0.250 nm. Of the 32 octahedral holes, 28 are pseudo-octahedral, distorted, and empty, whereas four are truly octahedral and each contains a Co atom in a formally zero oxidation state. Thus the solid attains the overall stoichiometry Co_9S_8 [4]. Figure 1 shows the conventional unit cell of Co_9S_8. The $\mathbf{Co_9S_8}$ has a space group *Fm3m*.

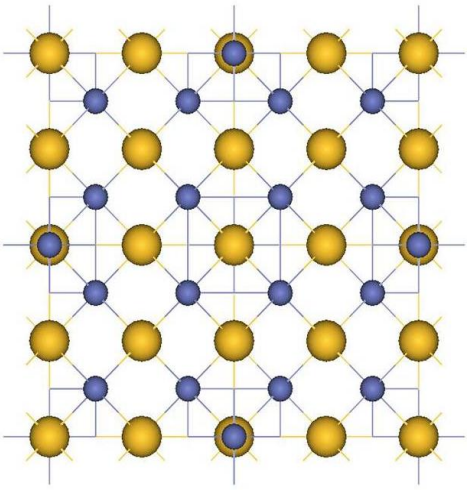

Figure 1: Conventional unit cell of cobalt pentlandite structure (Co_9S_8). Blue and yellow spheres represent cobalt (Co) and sulphur (S) atoms respectively.

2. Methodology

The VASP code [5] was used to calculate the elastic properties of Co_9S_8 (used as the existing data, for derivation of the interatomic potentials). Interatomic potentials of Co_9S_8 were derived by GULP [6] code and together with DLPOLY [7] molecular dynamics (MD) simulations were performed. The Born ionic model [8] was used and parameters were derived for short range interactions represented by the Buckingham potential, Morse potential and three body terms:

Buckingham Potential

In the Buckingham potential, the repulsive term is replaced by an exponential term and potential takes the form

$$U(r_{ij}) = A_{ij} * \exp^{-r_{ij}/\rho_{ij}} - \frac{C_{ij}}{r_{ij}^6} \qquad (1)$$

Where A_{ij} and ρ_{ij} are parameters that represent the ion size and hardness, respectively. The first term is known as the Born-Mayer potential and the attraction term was later added to form the Buckingham potential. Very often, for the cation-anion interactions, the attractive term is ignored due to the very small contribution of this term to the short-range potential, or, alternatively, the interaction is subsumed into the A and ρ parameters.

Morse Potential

The Morse potential is used to model the interactions between covalently bonded atoms and has the form

$$U(r_{ij}) = A_{ij} * (1 - \exp^{-B_{ij} * (r_{ij} - r_0)})^2 - A_{ij} \qquad (2)$$

where A_{ij} is the bond dissociation energy, r_0 is the equilibrium bond distance, and B_{ij} is a function of the slope of the potential energy well. The Coulombic interactions between covalently bonded atoms are often partially or totally ignored as the Morse potential already contains the attractive component of the interaction between neighbours.

Three-Body Potential

A further component of the interactions of covalent species is the bond-bending term, which is added to take into account the energy penalty for deviations from the equilibrium value. Hence, this potential describes the directionality of the bonds and has a simple harmonic form:

$$U(\theta_{ijk}) = \frac{1}{2} k_{ijk} (\theta_{ijk} - \theta_0)^2 \quad (3)$$

where k_{ijk} is the three-body force constant and θ_0 is equilibrium angle.

3. Results and Discussions

The properties, i.e. lattice parameters and elastic properties to validate the derived potential model of Co_9S_8 are discussed and also molecular dynamics simulation of bulk Co_9S_8 at high temperatures is discussed.

3.1. Validation of Potential Model of Co_9S_8

The accuracy of the derived interatomic potentials was checked by comparing the known experimental and calculated data. To validate our potential models we start by showing the properties that where obtained from our derived potentials i.e., lattice parameters and elastic properties. The lattice parameters obtained using energy minimisation code GULP is in good agreement with those from the literature as shown in Table 1.

Table 1. Comparison of the lattice parameter of Co_9S_8, obtained from the derived interatomic potentials, with the other calculated and experimental values.

Method	a (**Å**)
GULP (This work)	9.806
VASP (PW-GGA)(This Work)	9.811
*TB-LMTO[a]	9.918
Extended Huckel Type Band Calculations[b]	9.927
EXPERIMENTAL[c]	9.928

[a][10], [b][11], [c][9]

*Tight-binding linear-muffin-tin-orbital

Table 2 shows a comparison of the elastic properties of Co_9S_8 we calculated using DFT methods (VASP code) and those calculated from our derived interatomic potentials employing the GULP code; experimental elastic constants are currently not available for Co_9S_8. The elastic constants from the interatomic potentials are in good agreement with those from DFT calculations, together with the various moduli of elasticity, i.e. the bulk, shear, elasticity moduli and Poisson's ratio. In addition, the Co_9S_8 phase has elastic constants that satisfy the generalized elastic stability criteria for cubic crystals [12] [13]:

$$(C_{11} - C_{12}) / 3 > 0, C_{11} + 2C_{12} > 0, C_{44} > 0 \quad (4)$$

The bulk modulus *B*, shear modulus *G* and elastic modulus *E* of the cubic Co_9S_8 phase were deduced according to the following formulae [14] [15] [16] [17].

$$B = \frac{1}{3}(C_{11} + 2C_{12}) \quad (5)$$

$$G = \frac{1}{5}(C_{11} - C_{12} + 3C_{44}) \quad (6)$$

$$E = \frac{(C_{11} - C_{12} + 3C_{44})(C_{11} + 2C_{12})}{2C_{11} + 3C_{12} + C_{44}} \quad (7)$$

Poisson ratio v is obtained from:

$$v = \frac{3B - E}{6B} \quad (8)$$

Table 2. Calculated elastic constants and moduli of the Co_9S_8 phase

Properties	VASP	GULP (Fitted)
C_{11}	223.8	214.3
C_{12}	80.3	82.3
C_{44}	71.3	70.0
Bulk Modulus, *B* (GPa)	128.1	126.3
Shear Modulus, *G* (GPa)	71.5	68.4
Elastic Modulus, *E* (GPa)	180.8	173.8
Poisson Ratio, v	0.26	0.27
Volume (A^3) *		947.6

*Experimental Volume is 978.56 $Å^3$ [9]

3.2. Molecular Dynamics Simulation of Co_9S_8

In order to demonstrate the phase changes of the Co_9S_8 structure using molecular dynamics, we superimposed the total radial distribution functions of Co_9S_8 bulk at different temperatures in Figure 1. The total magnified RDFs indicate that as the temperature increases, the peaks become broader and the number of peaks decreased. Furthermore, the total RDFs show that between 300 and 900 K, the second and third peaks (denoted by B and C, respectively) are well-defined and approach each other. However, at 1100 K the peaks coalesce, and the combined peak (denoted by D) remains in the same position at 1300 K. This is the temperature range where Co_9S_8 undergoes phase change from normal to high form pentlandite according to experimental work of Kitakaze & Sugaki [18]. They reckoned that the high form of cobalt pentlandite is stable up to 930°± 3 °C (1203 K ± 3 K) , where it breaks down to a mixture of cobalt monosulfide (Fe- and Ni-free end-member of monosulfide solid-solution) and liquid in an incongruent melting reaction. They finally observed that, remnant cobalt monosulfide melts completely at 1069° ± 5 °C (1342 ± 5 K). Indeed our simulations (Figure 1) confirm the molten phase at 1500 K, since the height of the coalesced peak is reduced, which is further in agreement with the total energy versus temperature (Figure 4.4) anomalous enhancement above 1400 K. At a higher temperature of 1900 K the height of the coalesced peak is further reduced showing a completely molten structure. The first peak of the RDF gives a radial distance of approximately 2.15 Å at 300 up

to 900 K and 2.17 Å at 1100 K up to 1500 K. The radial distance is close to the experimental interatomic distance of Co-S on the tetrahedral site which is 2.13 Å. The second and third peaks give approximately 3.45 Å and 3.97 Å, respectively at 300 K up to 900 K. At 1100 K up to 1500 K the second and third peaks combine to give one peak of approximately 3.61 Å. The radial distance is close to the EXAFS measurement interatomic distance of Co-Co on the tetrahedral site which is 3.54 Å [18]. Hence it may be deduced that the phase change from the normal to high form pentlandite is associated with the movement of Co on the tetrahedral sites. The ability of the interatomic potentials to reproduce the complex high temperature phase change of pentlandite and to elucidate atoms participating in such change demonstrates the robustness of the potentials.

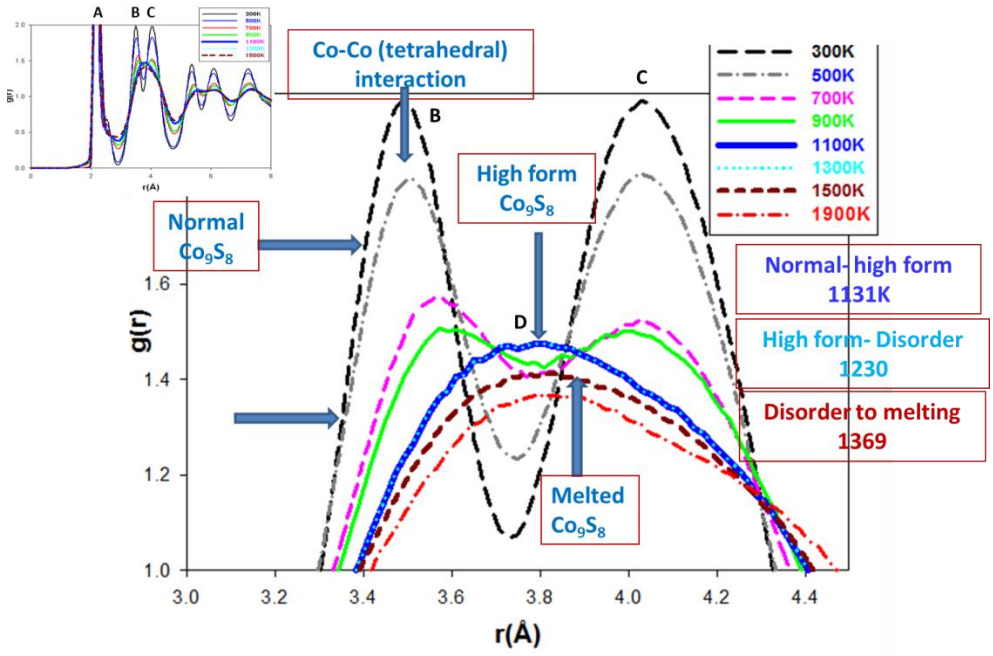

Figure 2: The total radial distribution functions of the Co_9S_8 bulk structure at different temperatures.

4. Conclusion

The derived interatomic potentials of Co_9S_8 were validated by the accurate determination of structure and elastic constants. The robustness of the interatomic potentials was further illustrated by their ability to reproduce complex high temperature transitions of the bulk Co_9S_8 which were observed experimentally. The change of radial distribution functions (especially the coalescing (coming together of the adjacent Co-Co tetrahedral peaks) deduced from molecular dynamics studies, depicted the phase change from the normal to the high form Co pentlandite above 1100K.

Acknowledgements

The computations were performed at the Materials Modelling Centre (MMC), University of Limpopo and at the Centre for High Performance Computing (CHPC). We also acknowledge the National Research Foundation (NRF) and Anglo Platinum for funding.

References

[1] Borodaev Y S, Bryzgalov I A, Mozgova N N and Uspenskaya T Y 2007 *Moscow Univ. Geol. Bull.* **62** 85-97

[2] Johan Z, Ohnenstetter M, Slansky E, Barron L M and Suppel D 1989 *Mineralogy and Petrology*, **40** 289-309

[3] Mehlape M A, 2013 *Computational Modelling Studies of Cobalt Pentlandite (Co_9S_8)*. (PhD Thesis, University of Limpopo)

[4] Hoodless R C, Moyes R B and Wells P B 2006 *Catalysis Today*, **114** 377–382

[5] Kresse G and Hafner J 1993 *Phys. Rev. B* **47** 558–561
[6] Gale J D 1997 *J. Chem Soc. Faraday Trans.* **93** 629
[7] Smith W and Forester T R 1996 *J. Mol. Graphics*, **14** 136-341
[8] M. Born and K. Huang, 1954 *Dynamical Theory of Crystal Lattices 1st edition* (University Press: Oxford)
[9] Geller S 1962 *Acta Crystallogr*, **15** 1195-1198
[10] Chauke H R, Nguyen-Manh D, Ngoepe P E, Pettifor D G and Fries S G 2002 *Phys. Rev. B,* **66** 155105-5
[11] Burdett J K and G J Miller 1987 *J. Amer. Chem. Soc.* **109** 4081-91
[12] Yu W, Wang N, Xiao X, Tang B, Peng L and Ding W 2009 *Solid State Sciences,* **11** 1400–07
[13] Dian-wu Z, Jin-shui L and Ping P 2011 *T. Nonferr. Metal. Soc.* **21** 2677−83
[14] Mehl M J, Osburn J E, Papaconstantopoulos D A and Klein B M 1990 *Phys. Rev. B: Condensed Matter,* **41** 10311−23
[15] Wang T, Chen P, Deng Y and Tang B, 2011 *Trans. of Nonferr. Metal Soc. of China,* **21** 388−394
[16] Screiber E, Anderson O L and Soga N, 1973 *Elastic constants and their measurement*, (McGraw-Hill, New York)
[17] Benkabou F, Aourag H and Certier M, 2000 *Mater. Chem. Phys.* **66** 10–16
[18] Kitakaze A and Sugaki A 2004 *Can. Mineral*, **42** 17-42
[19] Bouwens S M A M, Van Veen J A R, Koningsberger D C, De Beer V H J, and Prins R, 1991 *J. Phys. Chem.* **95** 134-139